

Multiphysics Design of High-Power Microwave Vacuum Window

Fabrizio Marrese¹, Lorenzo Valletti¹, Stefano Fantauzzi¹, Alberto Leggieri¹,
Mostafa Behtouei², Bruno Spataro², Franco Di Paolo¹

¹Università degli Studi di Roma “Tor Vergata”, Dipartimento di Ingegneria Elettronica Via del Politecnico, 1 – 00133 – Roma, Italy, fabrizio.marrese@gmail.com, lorenzo.valletti@uniroma2.it, stefano.fantauzzi@uniroma2.it, alberto.leggieri@uniroma2.it, franco.di.paolo@uniroma2.it

²Istituto Nazionale di Fisica Nucleare, Laboratori Nazionali di Frascati. P.O. Box 13, 00044, Frascati, Italy
mostafa.behtouei@lnf.infn.it, bruno.spataro@lnf.infn.it

Abstract— This paper presents the Multiphysics Analysis of a High-Power Microwave Window for a Ka-Band Klystron providing 16MW of peak power. After the optimization of the electromagnetic performances, we analyze the effect of RF heating effect and the stress of the pressure on the window. We also analyze the multipactor effect, that is a common cause of window failure. Using such approach, it is possible to realize a virtual prototype capable to represent in a complete way the real prototype to be manufactured.

Index Terms— High Power Microwaves, Klystron, Multipactor, Vacuum Tubes, Vacuum Windows.

I. INTRODUCTION

In this paper a microwave window for the output cavity of a Ka-Band Klystron has been designed and a virtual prototype has been proposed to evaluate the applicability of the proposed solution. Klystrons are high power microwave sources[1]–[3] usually used in radar, satellite and wideband high-power communication, medicine (radiation oncology), and high-energy physics (particle accelerators and experimental reactors). The proposed vacuum window is dedicated to the klystron solution for the “Compact Light XLS” project [4], where a short ultra-high gradient linearizer working on the third harmonic (36 GHz) with respect to the main linac frequency (11.988 GHz) operating with an accelerating gradient of 150 MV/m is requested. To provide the requested high-power signal, at Istituto Nazionale di Fisica Nucleare (INFN)-Laboratori Nazionali di Frascati (LNF), a 36GHz Klystron with a pulsed signal of 16MW of peak power with 200 ns pulse width and 10Hz of pulse repetition frequency was designed [5]. We assumed the characteristics of the INFN-LNF Klystron as the work specifications of the proposed vacuum window.

Microwave windows are critical components of High-Power Microwave Tubes since they limit the

maximum power handling capability of the device. Their purpose is to seal the tube vacuum atmosphere while ensuring the electromagnetic signal passes being forwarded to the output waveguide (that is placed under air or SF6 atmosphere) without major alterations. Usually, microwave windows are made of a ceramic disk brazed inside a waveguide on the output port of the tube. They must provide high power transfer and load matching condition, especially for high power application. The failures are often related to Electromagnetic dissipation on the volume of the window (Microwave Heating) and dielectric breakdown due to Single Surface Multipactor effect. Consequently, window Multiphysics design is a critical aspect in Klystrons, almost as much as resonant cavity design, of which [6] is a good example.

This paper is organized as follows. In section II, a brief of the chosen window type and substrate is given. In section III the electromagnetic characterization of the window is reported. In sections IV and V Thermal and Structural simulation are reported. Finally, in the last section Conclusions we summarize the results of this work.

II. WINDOW TYPE AND SUBSTRATE SELECTION

The proposed window is a pill-box type [7], as shown in Fig. 1, It is made of two sections of rectangular waveguide and a ceramic disk of alumina. Alumina Wesgo AL-300 has been chosen as the window ceramic material; the characteristics of this material are described in Table I.

TABLE I. ALUMINA WESGO AL-300

ϵ_R	$\tan\delta$	Dielectric Strength [MV/m]	Maximum Working Temperature [°C]	Thermal Conductivity [W/mK]	Compressive Strength [MPa]	Flexural Strength [MPa]	Purity [%]	Thermal Expansion Coefficient [1/K]	Joung Module [Pa]
9.04	0.0005	43	1650	26.7	1724	317	97.6	8.5e-6	300e9

The outer waveguides are WR28 type, while the inner one is a circular section where the ceramic window is brazed, this is the typical structure of a pill-box resonant cavity. The pill-box ends both sides with two circular to rectangular transitions, shown in Fig. 1.

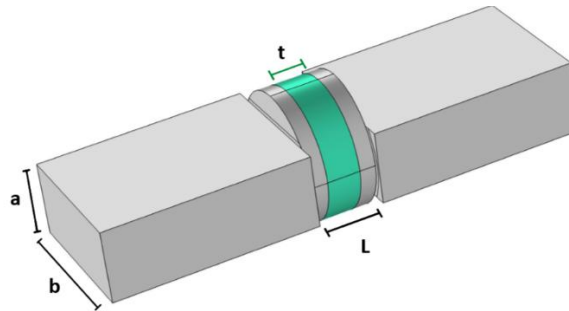


Fig. 1. Pill-Box window.

The design of this window is made according to procedure described in [1] resulting in pill-box length of $L=3.147\text{mm}$ and a radius of $r=3.255\text{mm}$.

The window thickness is $t=1.6\text{mm}$. The ceramic disk made with Alumina Wesgo AL-300 exhibits a purity of 97.6%. Dielectric constant is 9 and $\tan(\delta)=0.0005$.

III. ELECTROMAGNETIC SIMULATIONS

Simulations have been performed using HFSS to plot scattering parameters S_{21} and S_{11} nearby 36GHz which is the Klystron output frequency, to verify the modes inside the device and to check for ghost modes [8], [9].

In first instance, a modal analysis has been performed to verify monomodal propagation. Electromagnetic field boundaries have been set. It has been considered that all the waveguide surfaces were made of Perfect Electric Conductor (PEC) material and filled with air. Input and output electromagnetic ports have been arbitrarily chosen between the two rectangular terminations of the pill-box. The Real and Imaginary part of mode propagation constants are plot in Fig. 2, showing that the structure is monomodal between 21.5 GHz (cut-off) and 42.2 GHz (cut-off frequency for the second mode). At 36 GHz, which is in this range, the only mode in the rectangular waveguide is the TE_{10} which becomes TE_{11} in the circular one (Fig. 3).

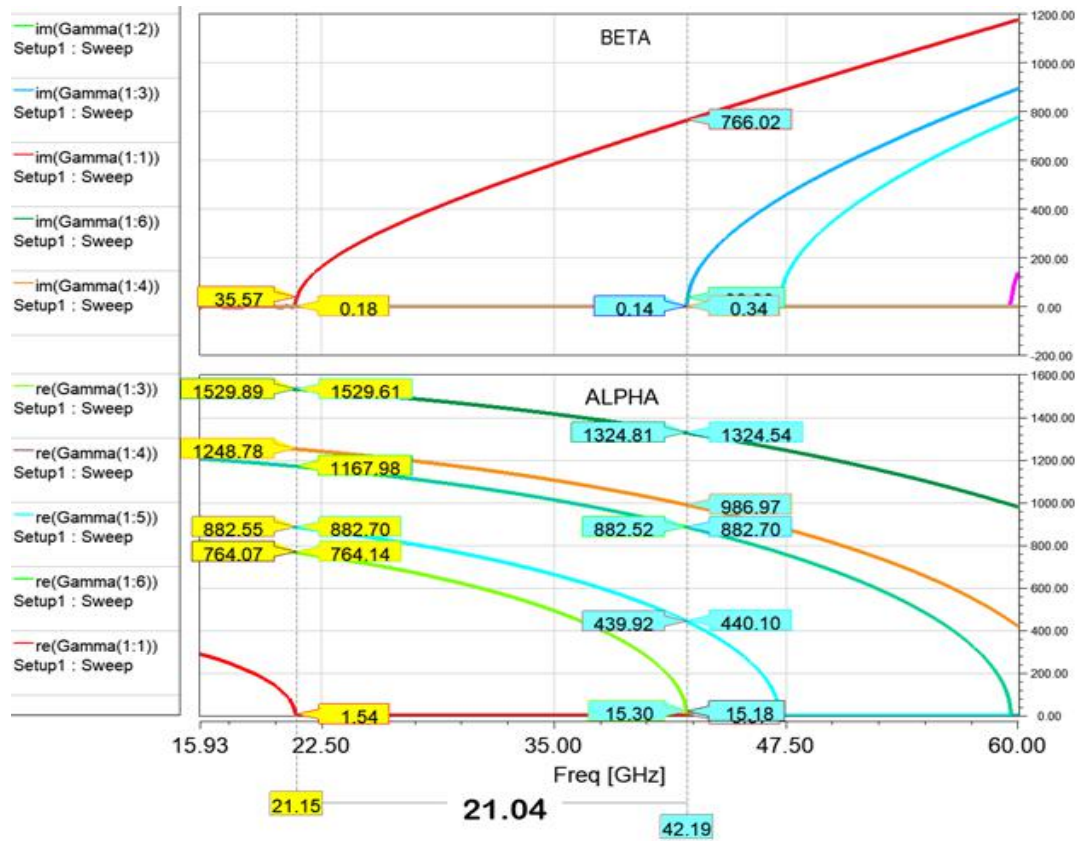


Fig. 2. Propagation constant plot of modes in the Window structure.

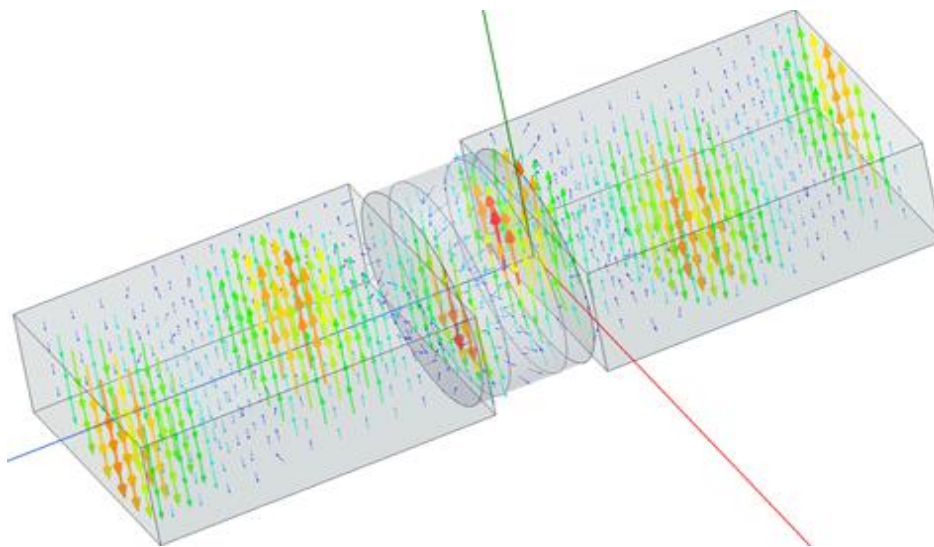


Fig. 3. Distribution of vector E inside the Window structure.

Then, in Fig. 4 the scattering parameters of the pill-box window are plotted respect to the first propagating mode. The figure shows that at 36 GHz, S_{11} is around -31 dB, while the S_{21} is -0.21.

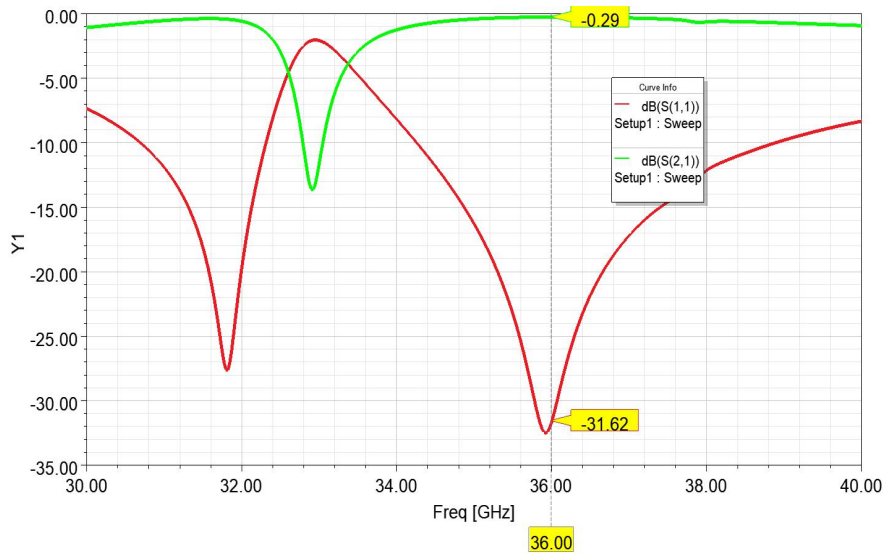


Fig. 4. Mode in the device.

The eigenmode simulation of the pill-box circular structure has been performed to investigate about ghost modes which could be excited in the structure. During eigenmode simulation, the input and output electromagnetic ports surfaces were closed considering them as PEC sheets, to permit a correct simulation. Some of the obtained eigenmodes are shown in Table II, where we can observe that the nearest mode to the klystron operative frequency is mode 15 at a frequency of 35.1857GHz which is 800 MHz below 36GHz; it's far enough from the operating frequency. Fig. 5 shows the electric field inside the window.

TABLE II. EIGENMODES OF THE PILL-BOX.

Eigenmode	Frequency (GHz)
Mode 11	32.966
Mode 12	32.97
Mode 13	33.05
Mode 14	33.05
Mode 15	35.186
Mode 16	37.848
Mode 17	37.85
Mode 18	37.92

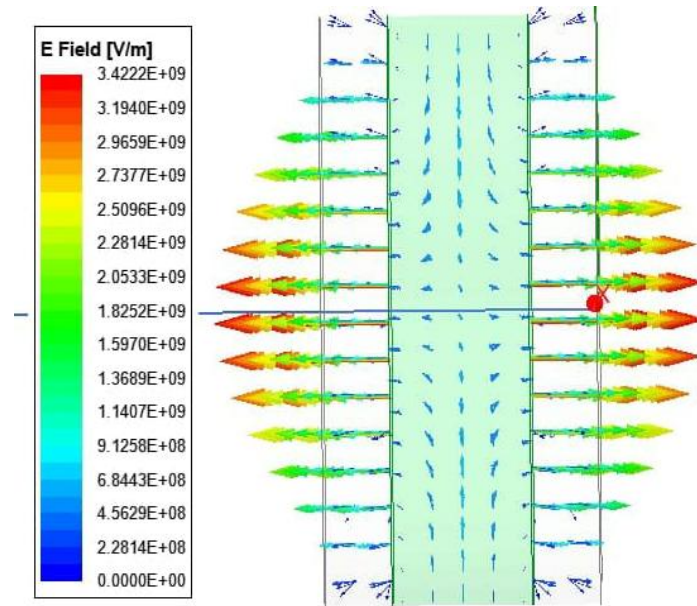


Fig. 5. Electric Field (Vector E) of mode 15 (35.186GHz).

IV. THERMAL SIMULATIONS

The window is subjected to thermal effects electromagnetic power dissipation on its volume. This phenomenon, called *microwave heating*, is strictly dependent on the distribution of the electric field on the window, so it depends on the mode propagating through the window. Power dissipated inside a volume V of material with imaginary dielectric constant ϵ'' is given by [10], [11]:

$$P = \frac{1}{2} \cdot \omega \cdot \iiint_{Volume} |E|^2 \cdot \epsilon_0 \cdot \epsilon'' \cdot dV \quad (1)$$

where E is the electric field, ω the angular frequency and ϵ_0 the vacuum dielectric constant. The thermal simulation has been performed in COMSOL Multiphysics to evaluate the average temperature reached by the dielectric crossed by electromagnetic field. The output signal of the Klystron is a pulsed signal with 16 MW peak, 200 ns of pulse duration (in the worst case) and 10pps (pulse per second). The RF Heating module of COMSOL Multiphysics has been used to perform the simulation in two steps: first, an electromagnetic simulation is done evaluating the electric field distribution and the power dissipated on the dielectric window, then this value is used by the “heat transfer in solids module” to simulate the heat flow from the window to the waveguide (by conduction), and from the waveguide to the outer environment (by convection). Heat dissipation by radiation has been neglected. In addition, the signal used in the first step is the Continuous Wave (CW) Equivalent of the Klystron pulsed operative signal, obtaining a 32W CW signal from the 16 MW peak power, pulse repetition interval 0.1s and 200 ns of pulse width pulsed signal, using the formula (2).

$$P_{avg} = \frac{P_{peak} \cdot \tau}{\Delta t} \quad (2)$$

where τ is the time duration of the pulse and Δt is the pulse repetition interval and P_{peak} is the peak power. In the used computational environment, the CW source as boundary condition (as a thermal source) allows to reduce the computational load of the simulation, compared to the case of a raw pulsed signal source. In the thermal simulation the CW signal is the heat source. It has been assumed that heat is generated exclusively in the dielectric window, setting an electromagnetic boundary condition on the waveguide walls, which have been set as PEC, so that electromagnetic power is not dissipate on them and totally reflected instead. This represents the worst-case scenario in the studying of the window heating. In regard of thermal boundaries, waveguide walls can absorb heat from the window through conductive heat exchange and they dissipate it through convective exchange to the air surrounding the structure.

The power dissipated in the ceramic material is about 19 kW but the time in which the dissipation take place is short, only 200ns, so the total energy dissipated per pulse is low.

The temperature results are shown in the Fig. 6, where the average temperature on the window's volume is plotted.

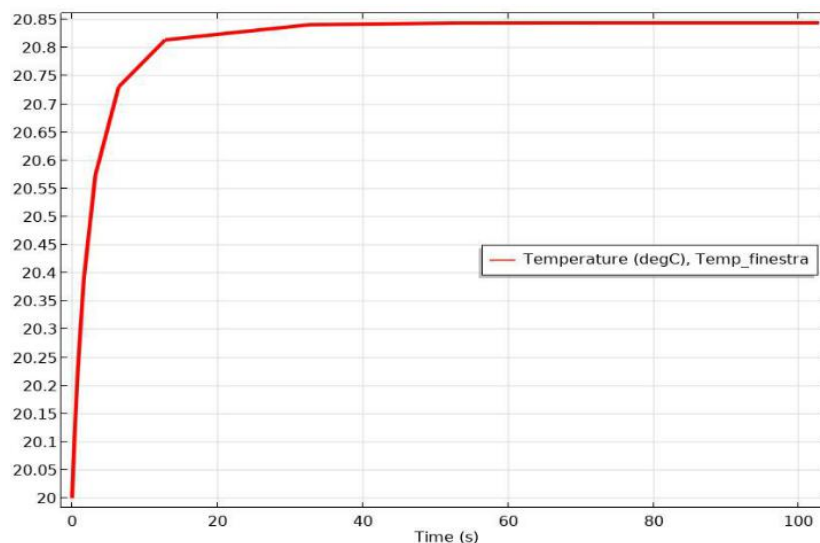


Fig. 6. Transient temperature simulation results: Average temperature.

After almost 40s the graph stabilizes since equilibrium is reached between the phenomenon of heat exchange. We recognize that microwave heating is a negligible phenomenon for our case of pulsed signals. In Fig. 7 are shown the electric field and the temperature distribution on the volume, verifying their dependency since the hottest area (in white) has the higher Electric Field module.

Finally, in Fig. 8 it is presented a simulation of the average temperatures reached by the window

depending on pps and τ (pulse width) with 16MW of peak power, with operational mode TE₁₀-TE₁₁.

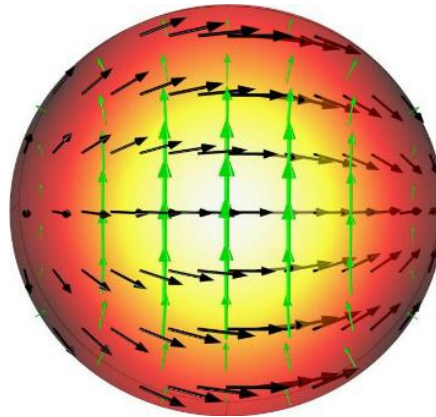


Fig. 7. TE₁₁ mode: (Green) Electric Field vectors, (Black) Magnetic Field vectors.

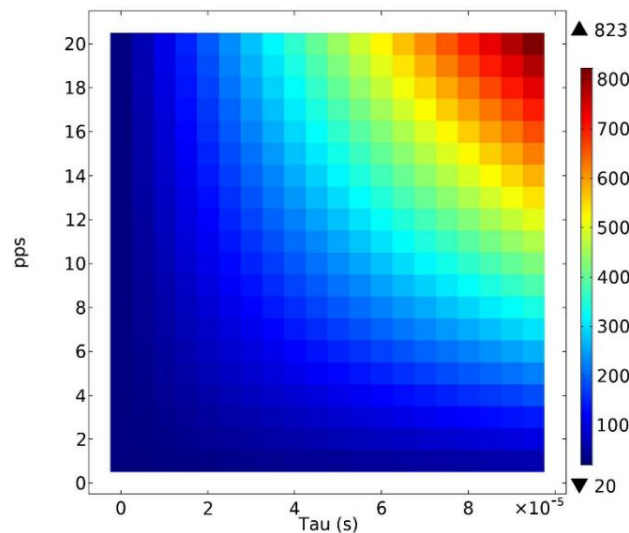


Fig. 8. Steady state average Temperature (K) chart.

The simulations for each point (pps, τ) has been performed with a steady-state simulation to simplify calculations.

V. STRUCTURAL SIMULATION

The window needs to seal the vacuum inside the tube, ensuring a vacuum pressure of 10^{-7} torr. So, it is subjected to a differential pressure between the two faces which compresses the air-side face, while the vacuum-side face is stretched. It has been performed a structural simulation with COMSOL Multiphysics to ensure that the maximum stress is lower than the maximum compressive and tensile stresses that the chosen material can manage before the breaking point. In the structural mechanics simulation, the curved surface of the cylindrical window has been chosen as a fixed boundary, while on the output and input circular sides are free to move and have been set at air pressure to 760 Torr

and vacuum pressure to 10^{-7} Torr.

In Fig. 9 it is shown the surface stress on the window while Fig. 10 is shown the stress along the diameters of the vacuum-side, air-side surfaces and of the middle section of the cylindrical window.

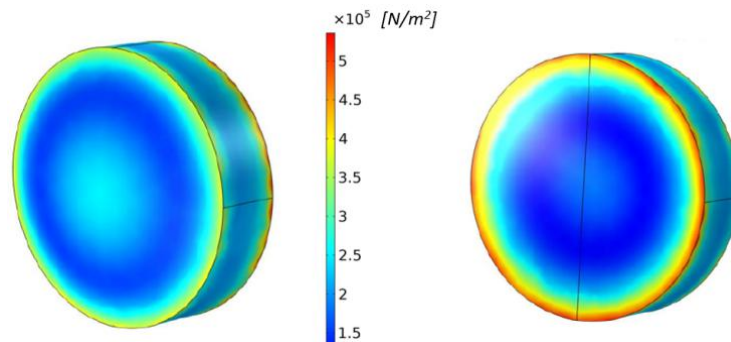


Fig. 9. Von Mises Stress on the surface.

As it can be extrapolated from the graphs, the maximum stress is located along the contact surface between the window and the waveguide at almost 0.85 MPa on the compressed side. This value is significantly lower than the maximum compressive strength of alumina Wesgo AL-300 (1724 MPa).

Finally, Fig. 11 illustrates the displacements along the previous diameters, which is maximum in the center of the structure and 0 on the border, where the window is fixed. The displacement is neglectable.

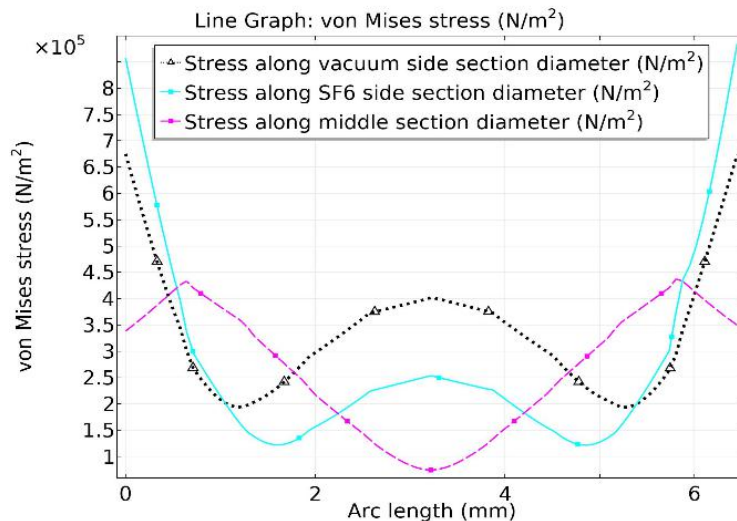


Fig. 10. Von Mises Stress on the outer surfaces' diameters.

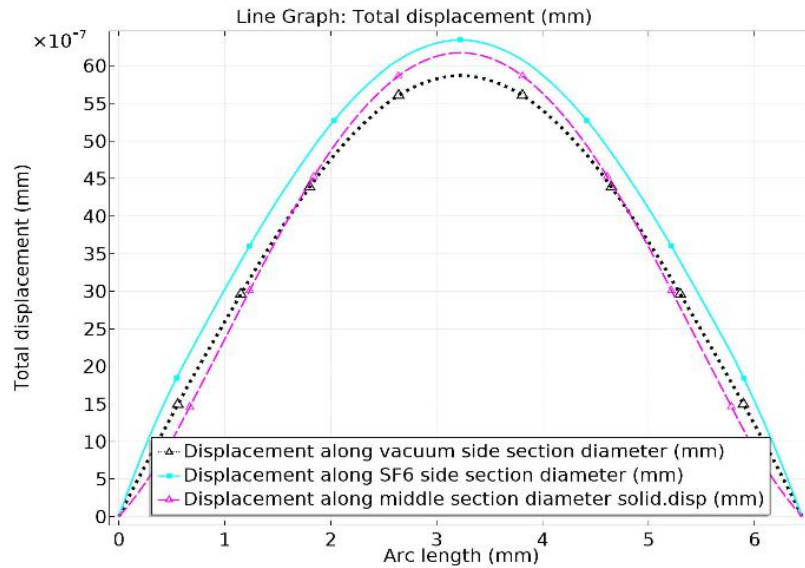


Fig. 11. Displacement curve.

To summarize, the noticeable squat shape of the window and the high values of maximum compressive and tensile strength of the chosen material, provide more than enough structural strength for the application.

VI. MULTIFACTOR ANALYSIS

Single Surface Multipactor effect is one the most common cause of window failure [12]–[14]. It is a phenomenon of free electron multiplication that take place near the vacuum-side surface of the window. It usually occurs when an electromagnetic field is propagating throughout the dielectric with an Electric Field component parallel to the surface with the presence of an external DC Electric Field perpendicular to it (Fig. 12).

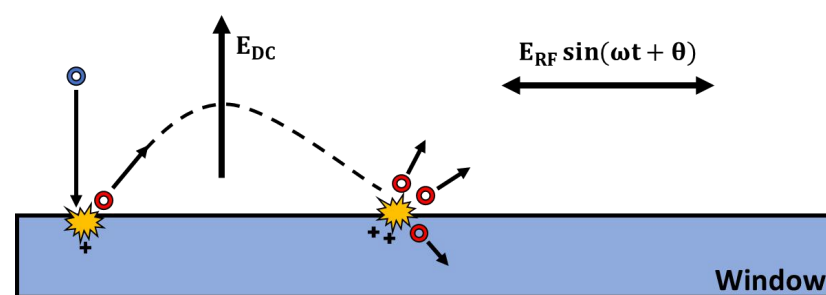


Fig. 12. Secondary Electron Emissions. The blue particle is a primary electron which impacts on the window surface extracting secondary electrons (in red). The DC field makes this particle return to the surface, while the phase of the RF field gives it enough energy to extract additional particles while it is absorbed back into the dielectric surface.

When a free (primary) electron impacts the surface there is a certain probability of extraction of one or more (secondary) electrons from the dielectric surface, which depends on the Secondary Electron Emission (SEE) yield of the material and the primary impact energy. Such emitted secondary electrons will eventually return to the dielectric surface due to the DC perpendicular Field, with an

energy that depends on the RF field. An avalanche effect occurs, triggering Multipactor, if the RF parallel field and the particle motion are in such synchrony that the former is able to supply sufficient energy to the latter to extract additional electrons. This phenomenon eventually saturates with a dynamic equilibrium between extracted and absorbed particles; a free electron cloud is formed nearby the dielectric surface and a positively charged region on the window, generated by the holes that secondary electrons left behind on the surface.

As explained in [15], Multipactor typically delivers on the order of one percent or less of the RF power onto the dielectric which in the case of a 16 MW peak power RF signal could lead to a 160 kW of power that could cause damage to the structure. The multipactor phenomenon may cause serious damage to the dielectric body of the window. The first effect is a steep increment of the temperature due to continuous electron bombardment on the dielectric surface, which is usually accompanied by light emission. That can cause surface located meltdown or cracks. In addition, the formation of a highly positively charged region on the window, due to the secondary electron extraction from the surface, could lead to dielectric breakdown and electrical discharge phenomenon, hence puncturing the structure.

So, multipactor simulations with CST-SPARK3D were performed to evaluate the possible entity of this phenomenon in the case of study.

The alumina secondary emission yield features have been extrapolated from 97.6% alumina graph [16], such as the peak point ($E_{\max}=750\text{eV}$, $SEY_{\max} = 5.6$), the low primary energy yield ($SEY_0 = 0.8$) and the first crossover energy ($E_1 = 25 \text{ eV}$). The results for the simulations have been reported in Fig. 13 showing how the number of free electrons sharply increases from 300 to almost a million in less than a nanosecond for 16 MW operating power.

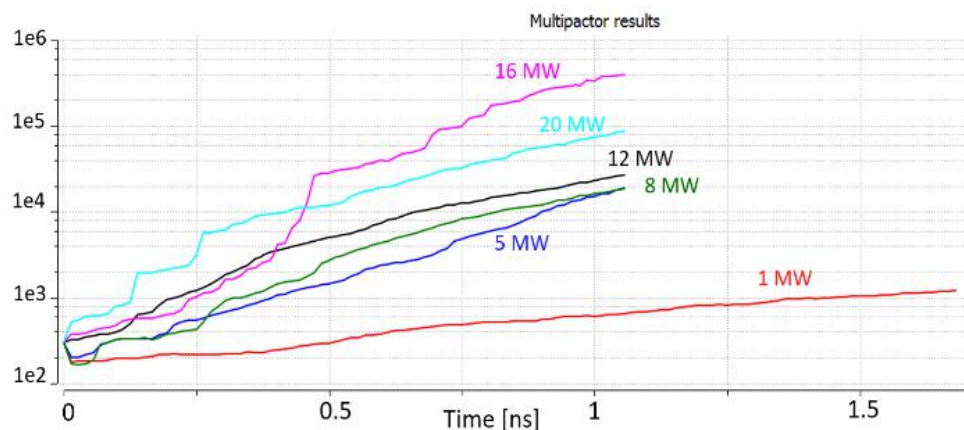


Fig. 13. Multipactor Results.

Furthermore, are presented the possible distribution of the particles during the multipactor phenomenon (Fig. 14) and the static Electric Field generated by them across the window (Fig. 16), which can lead to Dielectric Breakdown.

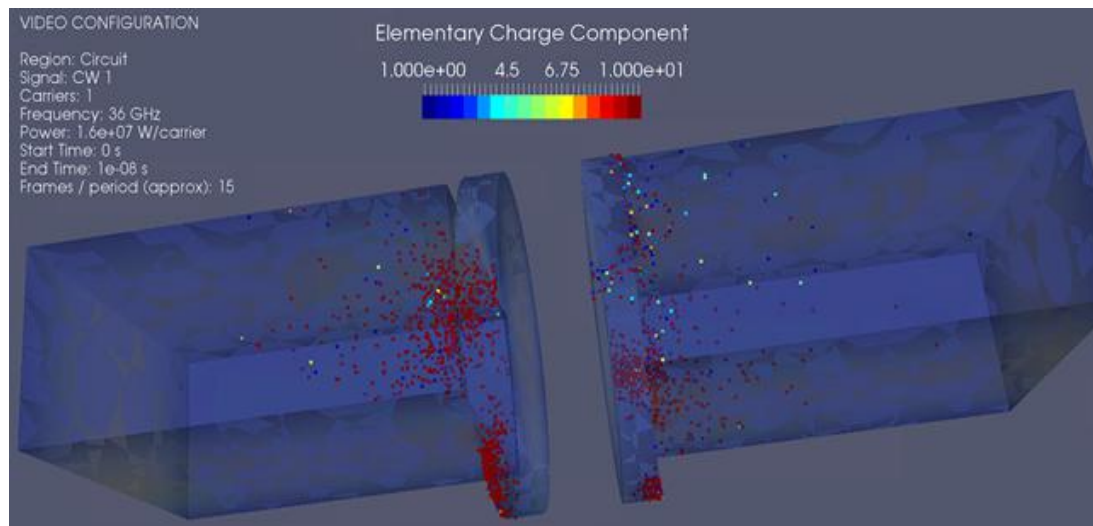


Fig. 14. Electron distribution during multipactor. The zones nearby the window in red are the most affected by multipactor.

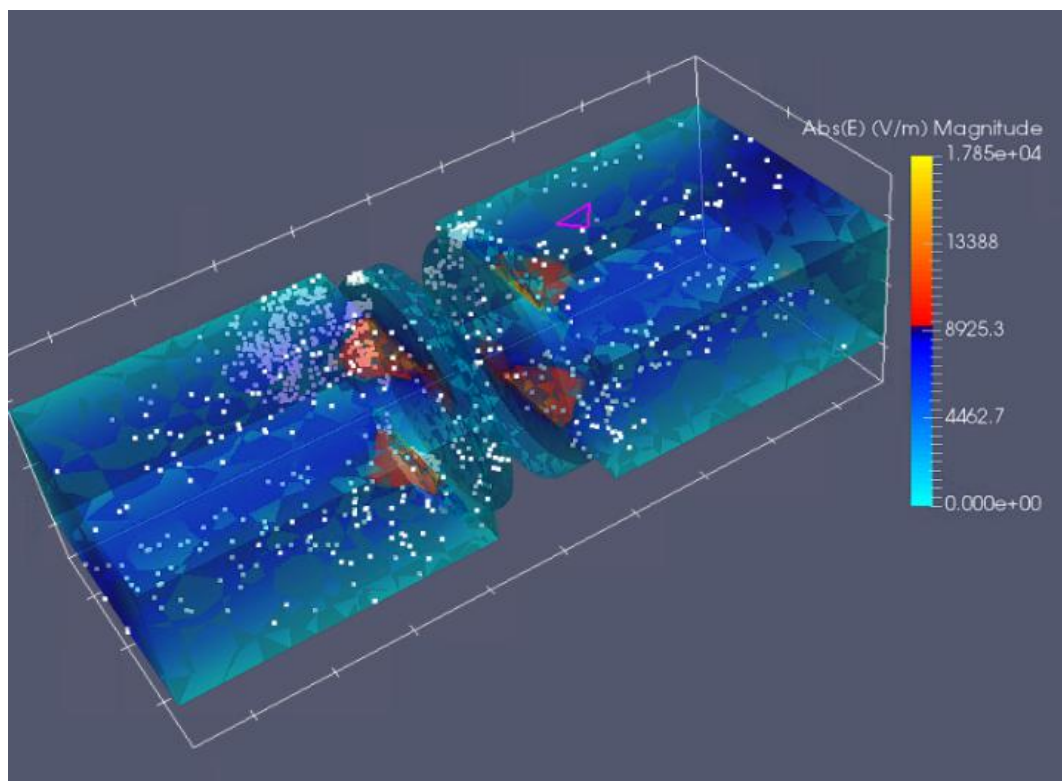


Fig. 16. Electric Field generated by multipactor.

In order to inhibit multipactor, it is possible to apply a TiN coating on the order of few nanometers of thickness, on the vacuum-side face of the dielectric window. TiN has a much lower SEE yield curve compared to the alumina one, so covering the windows with it significantly reduces the number of secondary electrons emitted after an impact thus, it reduces multipactor. Since TiN is a conductive material, coating the window with a TiN layer may short-circuit the whole structure, but it has been

proved how those extremely thin layers tend to form isolated and discontinuous structures so that the high conductivity of TiN does not affect the return loss of the window causing a short circuit [17], [18], while significantly reducing the SEE yield of the ceramic window [19].

VII. CONCLUSIONS

In this work, a complete multiphysics design approach has been considered to design a microwave window for pulsed high-power Klystron working at Ka-Band. Multipactor problems have also been analyzed and mitigated, since this phenomenon is often cause of window failures. At the Authors' best knowledge, it is the first time that such complete window numerical analysis and design is reported in literature. The proposed complete multiphysics analysis allows a virtual prototype of the window, capable to manufacture a real prototype with the highest accuracy and performances and mitigating the industrial risk.

The design reported in this work shows that the microwave window stimulated by a pulse of 200ns and 16MW of peak power does not show a significant increase in temperature, and it is able to withstand the stress and strain caused by vacuum. However, the harmful phenomenon of multipactor is present, but it is possible to avoid it by TiN Coating of microwave window.

REFERENCES

- [1] G. Caryotakis and M. Park, "High Power Klystrons : Theory and Practice at the Stanford Linear Accelerator Center *," pp. 0–138, 2005.
- [2] P. Tenenbaum, "A Brief Introduction to RF Power Sources Klystrons," *Uspas Desy*, pp. 1–10, 2003.
- [3] T. G. Lee, G. T. Konrad, Y. Okazaki, H. Yonezawa, and M. Watanabe, "The Design and Performance of a 150-MW Klystron at S Band," *IEEE Trans. Plasma Sci.*, vol. 13, no. 6, pp. 545–552, 1985, doi: 10.1109/TPS.1985.4316471.
- [4] "http://www.compactlight.eu/Main/HomePage."
- [5] M. Behtouei, B. Spataro, F. Di Paolo, and A. Leggieri, "The Ka-band high power klystron amplifier design program of INFN," *Vacuum*, vol. 191, no. December 2020, p. 110377, 2021, doi: 10.1016/j.vacuum.2021.110377.
- [6] Z. Zhang, J. Luo, and Z. Zhang, "Analysis and suppression of high-order mode oscillation in an S-band klystron," *IEEE Trans. Plasma Sci.*, vol. 43, no. 2, 2015, doi: 10.1109/TPS.2014.2384597.
- [7] A. Leggieri, A. Ciccotelli, G. Felici, L. Zappelli, D. Passi, and F. Di Paolo, "Tuned window for standing wave linear accelerators," *Prog. Electromagn. Res. Symp*, pp. 2421–2428, 2014.
- [8] E. T. Jaynes and M. P. Forrer, "Resonant Modes in Waveguide Windows," *IEEE Trans. Microw. Theory Tech.*, vol. 8, no. 2, pp. 147–150, Mar. 1960, doi: 10.1109/TMTT.1960.1124714.
- [9] E. T. Jaynes, "Ghost Modes in Imperfect Waveguides," *Proc. IRE*, vol. 46, no. 2, pp. 416–418, Feb. 1958, doi: 10.1109/JRPROC.1958.286913.
- [10] J. Anto and R. C. Thiagarajan, "Coupled Electromagnetic and Heat Transfer Simulations for RF Applicator Design for Efficient Heating of Materials," *Coupled Electromagn. Heat Transf. Simulations RF Appl. Des. Effic. Heat. Mater.*, pp. 1–5, 2012, [Online]. Available: http://www.comsol.com/paper/download/152829/thiagarajan_paper.pdf.
- [11] R. W. Pryor and D. Ph, "Modeling Dielectric Heating : A First Principles Approach," *Proc. 2015 COMSOL Conf.*, p. 5, 2015.
- [12] J. R. M. Vaughan, "Multipactor," *IEEE Trans. Electron Devices*, vol. 35, no. 7, pp. 1172–1180, 1988, doi: 10.1109/16.3387.
- [13] Y. Saito *et al.*, "Breakdown of alumina rf windows," *Rev. Sci. Instrum.*, vol. 60, no. 7, pp. 1736–1739, 1989, doi: 10.1063/1.1140942.
- [14] D. H. Preist and R. C. Talcott, "On the heating of output windows of microwave tubes by electron bombardment," *IRE Trans. Electron Devices*, vol. 8, no. 4, pp. 243–251, 1961, doi: 10.1109/T-ED.1961.14797.
- [15] L. K. Ang, Y. Y. Lau, R. A. Kishek, and R. M. Gilgenbach, "Power deposited on a dielectric by multipactor," *IEEE Trans. Plasma Sci.*, vol. 26, no. 3, pp. 290–295, 1998, doi: 10.1109/27.700756.
- [16] G. Reefman, "Secondary electron emission in alumina," 2019. doi: 10.13140/RG.2.2.34509.38888.
- [17] C. A. Neugebauer and M. B. Webb, "Electrical conduction mechanism in ultrathin, evaporated metal films," *J. Appl.*

- Phys.*, vol. 33, no. 1, 1962, doi: 10.1063/1.1728531.
- [18] L. Holland and J. Greenspan, "Vacuum Deposition of Thin Films," *J. Electrochem. Soc.*, vol. 104, no. 5, 1957, doi: 10.1149/1.2428554.
- [19] Suharyanto, S. Michizono, Y. Saito, Y. Yamano, and S. Kobayashi, "Secondary electron emission of TiN-coated alumina ceramics," *Vacuum*, vol. 81, no. 6 SPEC. ISS., 2007, doi: 10.1016/j.vacuum.2005.11.062.